Journal of Engineering and Applied Sciences 11 (3): 395-401, 2016
ISSN: 1816-949X

Shape-based Automated Classification of Subdural and Extradural Hematomas

[1, 2]Hau-Lee Tong, [2]Mohammad Faizal Ahmad Fauzi, [1]Su-Cheng Haw,
[1]Hu Ng, [1]Timothy Tzen-Vun Yap, [1]Chiung Ching Ho
[1]Faculty of Computing and Informatics, [2]Faculty of Engineering,
Multimedia University, 63100 Cyberjaya, Malaysia

Abstract: This study reports the classification of subdural and extradural hematomas in brain CT images. The major difference between subdural and extradural hematomas lies in their shapes, therefore eight shape descriptors are proposed to describe the characteristics of the two types of hematoma. The images will first undergo the pre-processing step which consists of two-level contrast enhancement separated by parenchyma extraction processes. Next, k-means clustering is performed to garner all Regions of Interest (ROIs) into one cluster. Prior to classification, shape features are extracted from each ROI. Finally for classification, fuzzy k-Nearest Neighbor (fuzzy k-NN) and Linear Discriminant Analysis (LDA) are employed to classify the regions into subdural hematoma, extradural hematoma or normal regions. Experimental results suggest that fuzzy k-NN produces the optimum accuracy. It manages to achieve over 93% correct classification rate on a set of 109 subdural and 247 extradural hematoma regions, as well as 629 normal regions.

Key words: Hematoma classification, computed tomography, image segmentation, CT, LDA

INTRODUCTION

In general, subdural hematomas are very similar to extradural hematomas. They are a type of bleeding that occurs within the skull but outside of the brain tissues. A tear in the vein or artery are the cause for most of subdural and extradural hematoma cases. Subdural hematoma is caused by the bleeding below the dura. Extradural hematoma, on the other hand, is generally located in the temporal area and is caused by the tear of the middle meningeal artery. In other words, subdural hematoma occurs closer to the brain while extradural hematoma occurs closer to the surface of the skin. Medical imaging techniques such as Computed Tomography (CT), Magnetic Resonance Imaging (MRI) and Ultrasound (US) which let the doctors to look into the human body to diagnose the medical condition are usually carried out to identify the hematomas.

Various methodologies for detecting or segmenting brain abnormalities or regions of interest have been developed using computer-aided techniques (Shi *et al*., 2011; Cheng *et al*., 2010a; Chalana and Kim, 1997; Cheng *et al*., 2010b; Joo *et al*., 2004; Chou *et al*., 2001; Tan *et al*., 2012; Cheng *et al*., 2007; Kesavamurthy and SubhaRani, 2006; Cosic and Loncaric, 1997; Matesin *et al*., 2001; Li *et al*., 2009; Hara *et al*., 2007; Chan, 2007; Liu *et al*., 2008; Tech and Korrapati, 2011; Tong *et al*., 2011). Hematoma detection is one of the emerging topics in brain abnormality detection. Kesavamurthy and SubhaRani (2006) proposed a semi-automatic hematoma and infarct detection system by using seeded region growing algorithm. Different from a hematoma, an infraction is a type of ischemic stroke caused by the blockage in the blood vessels supplying the blood to the brain. In their research, the seeds are initially fixed on the potential area of the hematoma and the region is iteratively grown to obtain the desired regions. For a fully automated detection of the abnormalities, a rule-based classification (Cosic and Loncaric, 1997; Matesin *et al*., 2001) grounded on the intensity, area and adjacent neighbor have been proposed to annotate the regions likes calcification, hemorrhage and stroke lesion. Similarly, Li *et al*. (2009) presented a knowledge-based classification on the mean intensity of hematomas.

Besides the adoption of prior knowledge for the classification, midline approach is adopted by Hara *et al*. (2007) for the detection of extradural and subdural hematomas. In their approach, midline is located based on the boundary of the skull. Another method proposed by Chan (2007) uses the left-right asymmetry to extract the intracranial hematomas. Other than these, Liu *et al*. (2008) adopted a Support Vector Machine (SVM) learning model for the hematoma slices detection. In their research, SVM with a linear kernel is used to classify the normal slices and hematoma slices. Besides, Ramana proposed a

Corresponding Author: Hau-Lee Tong, Faculty of Computing and Informatics, Multimedia University, 63100 Cyberjaya, Malaysia

perceptron based on feed forward neural netresearch (Tech and Korrapati, 2011) for the classification of the different types of hematomas. In their approach, the input parameters (location and shape) are fed into a neural netresearch for its classification.

In this study, we extend our previous researchs on detection of abnormal regions (Lee *et al*., 2008), hemorrhagic slice (Lee *et al*., 2011) and intracranial hemorrhages (Lee *et al*., 2011) by adopting new shape features and several classifiers to further distinguish and classify the hematomas into subdural or extradural. On CT scans, both types of hematoma exhibit similar characteristics: they have relatively high intensity values and found in similar location. Their shape characteristics however, is rather different, hence reliable shape features may be able to distinguish them. In this research, two datasets generated by different CT scanners from two collaborating hospitals are used to test the efficiency and feasibility of the proposed method.

MATERIALS AND METHODS

Overview of the proposed method: Our proposed system, as shown in Fig. 1, consists of four main stages which are preprocessing, clustering, feature extraction and classification. The purpose of the preprocessing stage is to enhance the visibility of the images and prepare the images better for the subsequent clustering and classification stages. Clustering is then applied to aggregate all potential hematoma regions into a single cluster based on their intensity. The clustering helps the classification process by filtering out the irrelevant regions that have relatively low intensity compared to the hematomas. Next, several shape features are extracted from each Region of Interest (ROI). Eventually, all the extracted features are channeled into the classifier to annotate the subdural and extradural hematomas.

Pre-processing: The pre-processing stage consists of two contrast enhancement processes.

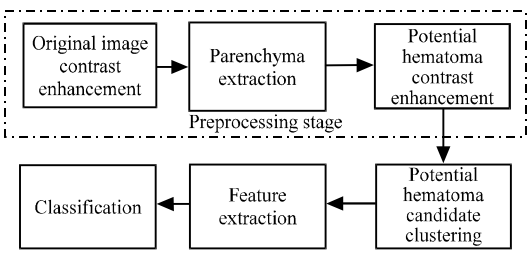

Fig. 1: Flowchart of the proposed system

Original image contrast enhancement: Without any contrast enhancement, the original images (an example is presented in Fig. 2a have very low visibility for the regions of interest (intracranial). Thus, an automatic-contrast enhancement method is proposed to improve the ROI's visibility. The images are subjected to the following steps:ZConstruct the histogram of the image. The histogram normally consists of two major peaks in which only the rightmost peak is contributed by the ROIs as depicted in Fig. 3a.

Smooth the histogram curve by convolving it with a vector which elements are having the value of 10^{-3} in order to obtain the distinct peaks. This is to aid the process of locating the upper and lower bounds. Transform the smoothened curve into absolute first derivative as shown in Fig. 3b.

Locate the upper bound I_U and lower bound I_L from the left and right peaks of the absolute first derivative as shown in Fig. 3b. I_U and I_L are the limits over which image intensity values will be extended linearly:

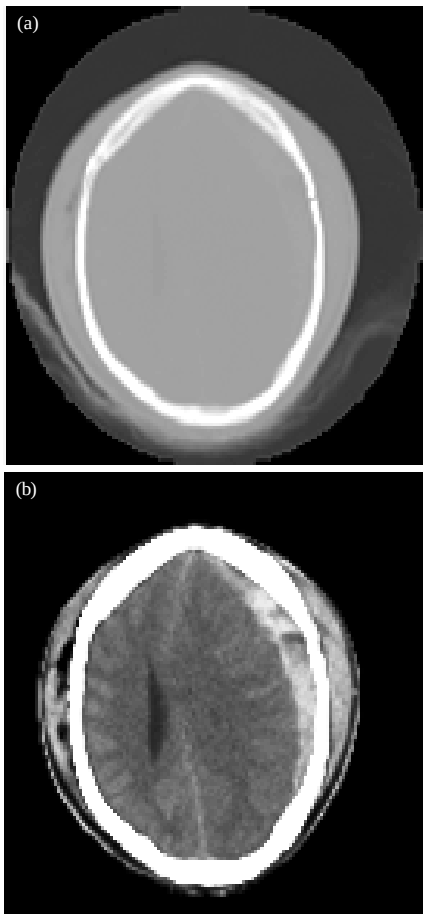

Fig. 2: The original and contrast refined image: a) original image and b) contrast refined image

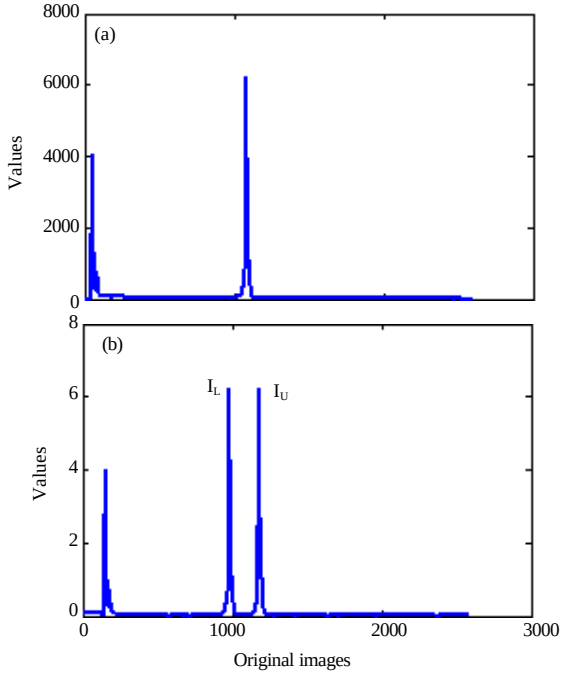

Fig. 3: Histogram of original image and its absolute first derivative: a) constructed histogram and b) absolute first derivative for (a)

$$F_{(i,j)} = I_{max}\frac{(I_{(i,j)}-I_L)}{(I_U-I_L)} \quad (1)$$

where, I_{max}, $I_{(i,j)}$ and $F_{(i,j)}$ denote the maximum intensity in the image, the original pixel intensity and the contrast enhanced pixel intensity, respectively. The contrast enhanced image for the example in Fig. 2a is shown in Fig. 2b. For all the images in our dataset, only two major peaks were encountered. Nevertheless, in case there are more than two major peaks, the algorithm will consider the two highest peaks on left and right.

Parenchyma extraction: After the contrast enhancement, thresholding is carried out to convert the image into binary. From experimental observations, all pixels values within the skull are found to be over 1700; hence, the threshold value is set at 1700. From the binary image, connected components analysis is performed to identify the largest blob which always appears to be the skull. Connected components analysis researchs by grouping the pixels into different components based on pixel connectivity with each component having a unique label. In our research, 8-connectivity is once the skull is identified, a commonly used flood-fill operation is done to fill up holes in the skull. Flood-fill operation searches for unmarked foreground pixel (value = 1) and then fills all the remaining neighboring pixels in its region. The skull is

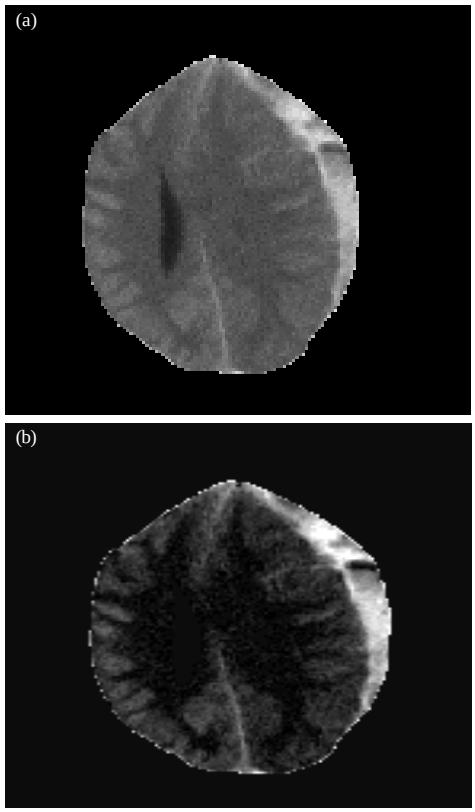

Fig. 4: Parenchyma and the enhanced image: a) Parenchyma and b) Enhanced image

then segmented out from the parenchyma by setting the intensity of the skull to zero to generate the parenchyma mask. The parenchyma obtained as shown in Fig. 4a.

Potential hematoma contrast enhancement: Generally, the intensity of the hematomas will fall after the peak position for the whole image. As such, the contrast of the hematomas can be enhanced by focusing on the higher side of the intensity. From the constructed histogram, the lower limit is automatically determined from the peak position of the histogram. The upper limit is then derived from the arithmetic operation:

$$I_U = I_l + I_a \quad (2)$$

where I_a is a step up intensity for obtaining the upper limit and is predefined at 500, obtained from experimental observation. The I_L and I_U are eventually channeled into Eq. 1 again for contrast stretching. The image after the contrast enhancement reduction is shown in Fig. 4b.

Potential hematoma candidate clustering: After the pre-processing, clustering is applied to partition the

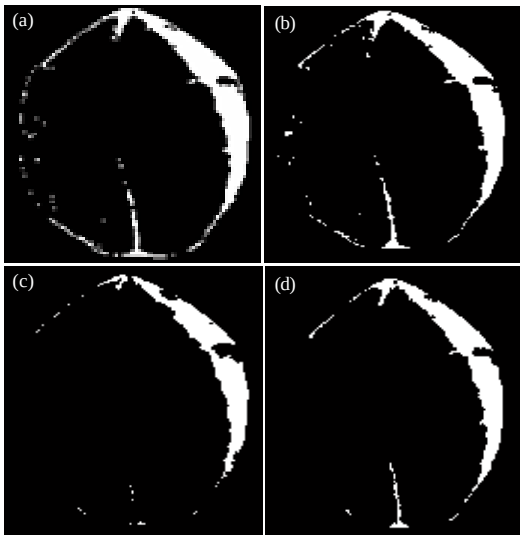

Fig. 5: Results of clustering by a) Otsu thresholding; b) FCM; c) K-means and d) EM

image into two segments. Basically, one of the segments consists of non-ROIs which have relative low intensity compared to the hematoma. The other segment, on the other hand, contains higher intensity regions which could be the hematomas themselves or some other regions with similar intensities to the hematomas. The segment which does not contain any potential hematoma regions will be omitted.

We have experimented with four clustering techniques which are Otsu thresholding, k-means clustering, Fuzzy C-Means clustering (FCM) and Expectation-Maximization Method (EM) in order to select the appropriate algorithm for the potential hematoma acquisition. Each of the four techniques was optimized before the comparison is made, in which they were iterated until it reaches the optimal results. Otsu thresholding exhaustively searches for different thresholds that minimize the intra-class variance. For k-means clustering, FCM clustering and EM method, the number of clusters is set to two and the iteration process is terminated when the error or misfit measure goes below the preset tolerance, 10^{-5}. An example of the comparison results for these clustering techniques is shown in Fig. 5.

From Fig. 5, it can be observed that Otsu thresholding, FCM clustering and EM clustering tend to merge more surrounding pixels with the hematoma to form a larger cluster. This over-segmentation problem causes the extradural and subdural regions to lose their unique shape characteristics. The results produced by k-means clustering, based on experiment on numerous images, produce less noise and preserves the actual shape of the hematomas most of the time. Based on this, k-means clustering is recommended to be used for the feature extraction and classification stages.

Feature extraction: Firstly, potential regions with similar intensity are transformed into binary images. From the binary images, several shape features are extracted from each connected component. Altogether, eight shape features are considered which are the region area, line of contact with the border, linearity, ellipticity, circularity, triangularity, Concavity and the Sum of Centroid Contour Distance Curve Fourier Descriptor (CCDCFD). The details of each feature are discussed as.

Region area: Region area measures the size of the region which is based on the number of pixels within the region. The region area is significant to isolate noisy pixels which tend to have similar intensity with the hematomas but with relatively much smaller sizes.

Line of contact: The use of line of contact is based on a priori knowledge that unlike the hematomas, some other abnormal regions such as falx, tentorium, etc., have less contact with the skull. We consider one of the adjacent neighbors of the subdural or extradural hematomas to be the skull. To obtain the line of contact, the potential regions are dilated by one unit. The line of contact is then defined as the intersection between the dilated area and skull.

Linearity: This descriptor measures the linearity (Stojmenovic *et al*., 2006) in the interval [0, 1] and is based on the ellipse-to-axis ratio. From the centroid of the ROIs, the first and second moments are obtained. The major and minor axes for the ROI can then be located and the linearity is defined as:

$$L(ROI) = 1-\frac{\text{minor axis}}{\text{major axis}} \quad (3)$$

Triangularity: This feature is derived based on moment invariants. Generally, extradural hematomas do not possess a perfect triangle shape. However, it has relatively high value of triangularity compared to other regions. The affine moment invariant used to characterise the triangle is given by:

$$I = \frac{\mu_{2,0}(ROI)\mu_{0,2}(ROI)-(\mu_{1,1}(ROI))^2}{(\mu_{0,0}(ROI))^4} \quad (4)$$

$$\mu_{i,j}(ROI) = \iint_{ROI} x^i y^j dxdy \quad (5)$$

From the affine moment invariant, the triangularity (Rosin *et al*., 2003) of an ROI is defined as:

$$\angle(\text{ROI}) = \begin{cases} 108I & \text{if } I \le \dfrac{1}{108} \\ \dfrac{1}{108I} & \text{otherwise} \end{cases} \quad (6)$$

Triangularity values range from [0, 1] and peaking at 1 when I = 1/108 where the ROI is a perfect triangle.

Ellipticity: The proper bi-convex extradural is in fact an ellipse with closed curve which is symmetric about its horizontal and vertical axes. To measure the ellipticity (Rosin *et al*., 2003) of a shape, similar approach to triangularity is used and is defined as:

$$\ell(\text{ROI}) = \begin{cases} 16\pi^2 I & \text{if } I \le \dfrac{1}{16\pi^2} \\ \dfrac{1}{16\pi^2 I} & \text{otherwise} \end{cases} \quad (7)$$

Circularity: To complement the ellipticity and triangularity in distinguishing extradural cases, circularity measure as proposed by Zunic *et al*. (2010) is defined by:

$$\partial(\text{ROI}) = \frac{(\mu_{0,0}(\text{ROI}))^2}{2\pi(\mu_{2,0}(\text{ROI}) + \mu_{0,2}(\text{ROI}))} \quad (8)$$

Concavity: This unique shape descriptor to measure the concavity of the hematomas, especially for subdural cases. It measures the degree of concaveness based on the subdural contour and the overlapping area. Several steps are required to measure the concavity as (using Fig. 6a as an example):

- Locate the non-contact contour with the skull and enclose it with a bounding box (Fig. 6b)
- Locate two appropriate points (x_1, y_1) and (x_2, y_2) from the non-contact contour that intersected with the bounding box. These two points are located based on nearest Euclidean distance from two different corners of the bounding box
- Based on (x_1, y_1) and (x_2, y_2), split the contours into inner (without contact with the skull (Fig. 6b) and outer contour (with contact with the skull (Fig. 6c)
- Acquire the closed contours for the inner and outer contour (Fig. 6d, e) by interpolation
- Apply the flood-fill operation to fill up both closed contours (Fig. 6f, g)
- Overlap the filled inner contour with the filled outer contour. The resulting overlapping region is as shown in Fig. 6h

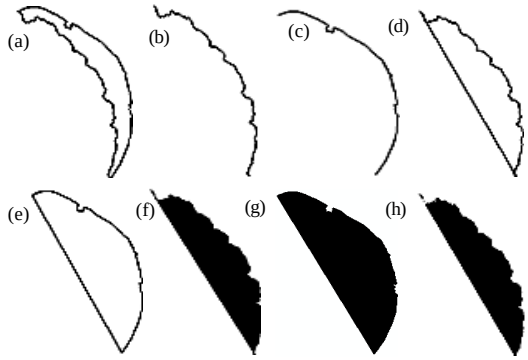

Fig. 6: Steps taken in measuring concavity: a) subdural region; b) inner contour; c) outer contour; d) inner closed contour; e) outer closed contour; f) filled up inner contour; g) Filled up outer contour and h) overlapping area

The concavity is defined as the ratio between the overlapping regions with the filled outer contour area. Note that the values are normalized to the range [0, 1].

Sum of Centroid Contour Distance Curve Fourier Descriptor (CCDCFD) --CCDCFD is another feature proposed to describe the subdural and to distinguish it from the extradural hematomas. The CCDCFD sum reflects the symmetry of the hematoma shapes. The more symmetric the shape, the lower the CCDCFD sum is. In computing the sum, we only consider the first 32 Fourier coefficients, due to the fact that most of the contour information is concentrated at the low frequency region. Dividing the coefficients with the second coefficient will normalize the range of the CCDCFD sum to [0, 1].

Classification: For the classification, two methods are considered which are Linear Discriminant Analyses (LDA) and fuzzy k-Nearest Neighbor (fuzzy k-NN). LDA projects data into a lower dimensional space. The optimal projection is accomplished by minimizing intra-class distance while maximizing the between-class distance. This generates optimal class separability.

On the other hand, Fuzzy k-NN is based on the identification of the k-nearest neighbors in the feature space. The relationship between the training and testing data is determined by the fuzzy membership function. Integration of the fuzzy membership function with k-NN reduces the bias of the classification for certain classes.

RESULTS AND DISCUSSION

The CT brain images were collected from 23 patients diagnosed with hematomas from our two collaborating partners, Hospital Serdang and Hospital Putrajaya. The gold standard of diagnosis was achieved based on the

radiologists' reports. Overall, there are 356 hematoma regions, out of which 109 are subdural and 247 are extradural cases. Besides, 629 normal regions but with similar intensities as hematomas were also extracted from the images to evaluate the algorithm's ability to reduce false positives.

The classification results were evaluated using ten-fold cross validation. The classification accuracy, the false positive rate and false negative rates for all the 985 regions generated from LDA classifier and fuzzy k-NN classifier are summarized in Table 1. As can be observed from the table, the chosen features generate satisfactory classification results with 79.39% accuracy for LDA and 93.60% accuracy for fuzzy k-NN. It was also observed that fuzzy k-NN outperforms LDA for all values of k from 2-20, with the optimum accuracy recorded when k = 8. The better performances of fuzzy k-NN could be contributed to the fact that the data are non-linearly separable. Besides, fuzzy k-NN gives the optimum rates for both false negative and false positive. The reporting of false negative and false positive rates is significant to reflect the amount of normal regions misclassified as hematomas and vice-versa and fuzzy k-NN is better at distinguishing these.

Besides the overall classification, accuracy for each class is also investigated. It can be seen from Table 1 that for both classifiers, classification accuracy for extradural cases is higher than subdural. This may be due to the fact that subdural hematomas are more irregular in shape and is thus more difficult to distinguish from the normal regions. It can also be observed that the LDA produced much lower accuracy compared to fuzzy k-NN classifier in classifying normal regions (76.63 vs. 95.23%). It can be concluded that the proposed shape features researchs very well with fuzzy k-NN classifier.

CONCLUSION

We have proposed a new shape features for the classification of brain hematomas into subdural and extradural categories, as well distinguishing them from normal regions. This is an extension to our previous researchs which focused on detecting abnormal regions and classifying the regions or slices into normal or hemorrhagic slice. Based on the experiments on two different datasets from two collaborating hospitals, the proposed system produced promising results with 93.60% overall accuracy recorded using fuzzy k-NN classifier and 79.39% overall accuracy using linear discriminant analysis. Fuzzy k-NN also outperforms LDA on each of the subdural, extradural and normal categories. Future researches will be directed towards the classification of more abnormalities in the brain such as infarct, atrophy and others.

REFERENCES

Chalana, V. and Y. Kim, 1997. A methodology for evaluation of boundary detection algorithms on medical images. IEEE Trans. Med. Imaging, 16: 642-652.

Chan, T., 2007. Computer aided detection of small acute intracranial hemorrhage on computer tomography of brain. Comput. Med. Imag. Graphics, 31: 285-298.

Cheng., J.Z., C.M. Chen, Y.H. Chou, C.S. Chen, C.M. Tiu and K.W. Chen, 2007. Cell-based two-region competition algorithm with a map framework for boundary delineation of a series of 2D ultrasound images. Ultrasound Med. Biol., 33: 1640-1650.

Cheng, J.Z., Y.H. Chou, C.S. Huang, Y.C. Chang and C.M. Tiu *et al*., 2010a. ACCOMP: Augmented cell competition algorithm for breast lesion demarcation in sonography. Med. Phys., 37: 6240-6252.

Cheng, J.Z., Y.H. Chou, C.S. Huang, Y.C. Chang, C.M. Tiu, K.W. Chen and C.M. Chen, 2010b. Computer-aided us diagnosis of breast lesions by using cell-based contour grouping. Radiology, 255: 746-754.

Chou, Y.H., C.M. Tiu, G.S. Hung, S.C. Wu, T.Y. Chang and H.K. Chiang, 2001. Stepwise logistic regression analysis of tumor contour features for breast ultrasound diagnosis. Ultrasound Med. Biol., 27: 1493-1498.

Cosic, D. and S. Loncaric, 1997. Rule-based Labeling of CT Head Image. In: Artificial Intelligence in Medicine, Keravnou, E., C. Garbay, R. Baud and J. Wyatt (Eds.). Springer, Berlin, Heidelberg, ISBN: 978-3-540-62709-8, pp: 453-456.

Hara, T., N. Matoba, X. Zhou, S. Yokoi and H. Aizawa *et al*., 2007. Automated detection of extradural and subdural hematoma for contrast-enhanced CT images in emergency medical care. Proc. SPIE, Vol. 6514. 10.1117/12.710307

Joo, S., Y.S. Yang, W.K. Moon and H.C. Kim, 2004. Computer-aided diagnosis of solid breast nodules: Use of an artificial neural network based on multiple sonographic features. IEEE Trans. Med. Imaging, 23: 1292-1300.

Kesavamurthy, T. and S. SubhaRani, 2006. Pattern classification using imaging techniques for infarct and hemorrhage identification in the human brain. Calicut Med. J., Vol. 4.

Lee, T.H., M.F.A. Fauzi and R. Komiya, 2008. Segmentation of CT brain images using K-means and EM clustering. Proceedings of the Fifth International Conference on Computer Graphics, Imaging and Visualisation, August 26-28, 2008, Penang, Malaysia, pp: 339-344.

Lee, T.H., M.F.A. Fauzi and S.C. Haw, 2011. Intracranial hemorrhage annotation for CT brain images. Int. J. Adv. Sci. Eng. Inform. Technol., 1: 689-693.

Li, Y., Q. Hu, J. Wu and Z. Chen, 2009. A hybrid approach to detection of brain hemorrhage candidates from clinical head CT scans. Proceedings of the 6th International Conference on Fuzzy Systems and Knowledge Discovery, Volume 1, August 14-16, 2009, Tianjin, pp: 361-365.

Liu, R., C.L. Tan, T.Y. Leong, C.K. Lee and B.C. Pang *et al*., 2008. Hemorrhage slices detection in brain CT images. Proceedings of the 19th International Conference on Pattern Recognition, December 8-11, 2008, Tampa, Florida, USA., pp: 1-4.

Matesin, M., S. Loncaric and D. Petravic, 2001. A rule-based approach to stroke lesion analysis from CT brain images. Proceedings of the 2nd International Symposium on Image and Signal Processing and Analysis, June 19-21, 2001, Pula, Croatia, pp: 219-223.

Rosin, P.L., 2003. Measuring shape: Ellipticity, rectangularity and triangularity. Mach. Vision Applic., 14: 172-184.

Shi, F., D. Shen, P.T. Yap, Y. Fan and J.Z. Cheng *et al*., 2011. CENTS: Cortical enhanced neonatal tissue segmentation. Hum. Brain Mapping, 32: 382-396.

Stojmenovic, M., A. Nayak and J. Zunic, 2006. Measuring linearity of a finite set of points. Proceedings of the IEEE Conference on Cybernetics and Intelligent Systems, June 7-9, 2006, Bangkok, pp: 1-6.

Tan, T., B. Platel, H. Huisman, C.I. Sanchez, R. Mus and N. Karssemeijer, 2012. Computer-aided lesion diagnosis in automated 3-D breast ultrasound using coronal spiculation. IEEE Trans. Med. Imaging, 31: 1034-1042.

Tech, K.R.M. and R.B. Korrapati, 2011. Neural network based classification and diagnosis of brain hemorrhages. Int. J. Artif. Intell. Exp. Syst., 1: 7-25.

Tong, H.L., M.F.A. Fauzi and S.C. Haw, 2011. Automated Hemorrhage Slices Detection for CT Brain Images. In: Visual Informatics: Sustaining Research and Innovations, Zaman, H.B., P. Robinson, M. Petrou, P. Olivier, T.K. Shih, S. Velastin and I. Nystrom (Eds.). Springer, Berlin, Heidelberg, ISBN: 978-3-642-25190-0, pp: 268-279.

Zunic, J., K. Hirota and P.L. Rosin, 2010. A Hu moment invariant as a shape circularity measure. Pattern Recognition, 43: 47-57.